Vortex-Wake-Blade Interaction in a Shrouded Axial Turbine

J. Schlienger[1]
e-mail: joel.schlienger@ch.abb.com

A. I. Kalfas

R. S. Abhari

Turbomachinery Laboratory,
Swiss Federal Institute of Technology,
Sonneggstrasse 3,
8092 Zurich, Switzerland

This paper presents time-resolved flow field measurements at the exit of the first rotor blade row of a two stage shrouded axial turbine. The observed unsteady interaction mechanism between the secondary flow vortices, the rotor wake and the adjacent blading at the exit plane of the first turbine stage is of prime interest and analyzed in detail. The results indicate that the unsteady secondary flows are primarily dominated by the rotor hub passage vortex and the shed secondary flow field from the upstream stator blade row. The analysis of the results revealed a roll-up mechanism of the rotor wake layer into the rotor indigenous passage vortex close to the hub endwall. This interesting mechanism is described in a flow schematic within this paper. In a second measurement campaign the first stator blade row is clocked by half a blade pitch relative to the second stator in order to shift the relative position of both stator indigenous secondary flow fields. The comparison of the time-resolved data for both clocking cases showed a surprising result. The steady flow profiles for both cases are nearly identical. The analysis of the probe pressure signal indicates a high level of unsteadiness that is due to the periodic occurrence of the shed first stator secondary flow field. [DOI: 10.1115/1.1934263]

Introduction

In recent years of turbine flow research, great importance is given to the time-varying flow field and the related generation of unsteady loss in a blade row. Denton [1] identifies different sources of loss for shrouded axial turbines. One source of loss is generated in the endwall flow field, when the leakage flow interacts with the main flow field and the endwall's secondary flow vortices. This mechanism is one reason for the reduction of the blade loading and the stage performance. The detailed unsteady flow measurement and the understanding of the flow physics is thus a key requirement in achieving further improvements of turbine efficiency.

The relative motion between the rotating and stationary turbine blades causes the rotor indigenous secondary flow and potential flow field, that is induced by the rotor and stator blades, to periodically interact with each other (Sharma et al. [2]). The evolution and convection of the stator and rotor hub vortices and wakes through the downstream blade rows are therefore triggered by the instantaneous relative position of the rotor and stator blades. The associated unsteady flow effects, that originate in the interaction of the wake with the secondary flow vortices and the blade geometry, contributes to a large extent to the generation and redistribution of unsteady loss. The convection of the upstream stator flow field through the downstream rotor passage is explained in the work of Miller et al. [3]. The shed stator vortices influence the formation of the rotor indigenous hub passage vortex as seen from numerical simulations.

The mechanism of the wake-blade interaction has been reported in several publications (including Hodson [4]) and is generally important for high aspect ratio and high lift airfoils as used in low pressure turbines. Major contributions in the field of unsteady vortex-blade interactions for unshrouded single or 1.5 stage turbines are found in the work of Binder et al. [5], Boletis and Sieverding [6], and Sharma et al. [2]. However, only a few publications report on the time-resolved vortex-blade interaction mechanism for a shrouded single stage turbine (i.e., Chaluvadi et al. [7] or Behr et al. [8]). The unsteady interaction of a vortex with a stationary blade row is experimentally investigated in Chaluvadi et al. [9] using delta wings as vortex generators at the hub inlet of a single stage turbine. The influence of an upstream rotor trailing edge on this mechanism is, however, not included in this experiment and needs some further investigations.

The paper focuses on the interaction of the rotor hub vortices with the rotor wake and the downstream stator leading edge of a two stage shrouded axial turbine. The associated unsteady variation of the relative total pressure, incidence angles and level of unsteadiness is analyzed and discussed in detail.

The unsteady flow field is ideally measured by detailed time-resolved flow field measurements using miniature fast response aerodynamic pressure probes (FRAP) Kupferschmied [10]. The high aspect ratio of 10:1 between the blade minimal throat and the head diameter of the fast response probe leads to a minimal blockage effect of the probe shaft within the measured flow field. Finally, the measurement technique provides the fully three dimensional time-resolved flow field of the turbine.

The results are presented as contour plots for the relative total pressure at different time steps and in combination with the derived secondary flow velocity vectors. The evolution of the flow profiles (e.g., relative total pressure) is given as pitchwise mass-averaged space–time diagrams and explained in detail.

In the work of Chaluvadi et al. [7], the turbulence level was measured with hot-wire probes and used as a marker for the generation of loss in a turbine stage. In the present study, the stochastic fluctuations of the dynamic head, that is measured with the fast response probes, is expressed as turbulence level, as proposed in the work of Ruck [11] and Koeppel [12] for fast response pneumatic probe techniques.

Experimental Method

Research Facility. The measurements were performed in the low speed two stage axial research turbine at the Turbomachinery Laboratory of the ETH Zurich (Fig. 1, Schlienger [13]). The rig consists of an axial turbine, a closed loop duct system, a radial compressor, a water/air cooler and a venturi nozzle for accurate massflow measurements within ±0.5% accuracy of the overall mass flow. The delivered turbine power is absorbed by a DC generator, that accurately controls the rotor speed within ±1 rpm.

The turbine is operated at a constant pressure difference across the two stages. The inlet temperature is kept constant at 45°C and varies within ±0.2°C over one day. The specific turbine operating

[1]Presently at: ABB Turbosystems, Baden, Switzerland.

Contributed by the Turbomachinery Division of THE AMERICAN SOCIETY OF MECHANICAL ENGINEERS for publication in the JOURNAL OF TURBOMACHINERY. Manuscript received by the ASME Turbomachinery Division August 11, 2004; final revision received February 21, 2005. Associate Editor: D. Wisler.

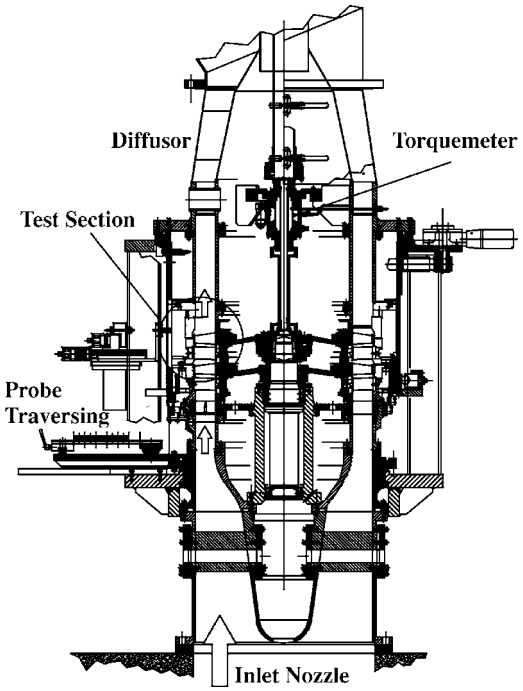

Fig. 1 Low speed 2-stage axial turbine LISA

point is given in Table 1. The pressure drop is stable to within ±40 Pa (±0.1% of total pressure drop) for a typical measurement time of one day.

The airfoil design is typical as for modern gas turbines. The moderate blade aspect ratio of 1.8, in combination with the labyrinth leakage flow field, enhances the secondary flow effects in the endwall area which leads to an averaged typical flow pitch angle of up to 20 deg. A set of highly sophisticated fast response pressure probes are required for the detailed measurements of this complex unsteady three-dimensional flow.

Probe Technology. The unsteady flow field is measured with two single sensor fast response aerodynamic pressure probes at a sampling frequency of 200 kHz (Kupferschmied et al. [10]). In this case, the FRAP probes are used as a pair in virtual 4-sensor mode for the measurements of the 3D time-resolved flow field. The measured flow parameters are the flow yaw (α) and pitch (β) angles, the total and static pressure coefficients (C_{pt} and C_{ps}) and the Mach number (Ma) at frequencies of up to 20 kHz. The measurement accuracy is given for Table 2 for the different probes that are used for this experiment.

A trigger signal, with a measured accuracy of ±1/108 of blade pitch, relates the four consecutive FRAP probe pressure measurements in space and time. The local flow vector is then reconstructed from those four pressures at each spatial coordinate using the aerodynamic probe calibration model. The raw data is phase-lock averaged using 80 rotor passing events and the rotor trigger reference signal. The obtained raw data files of the FRAP probe measurements are processed with the software program HERKULES (Schlienger [13]). The code is based on the Matlab programming language syntax. The overall processing time for 700 grid points per blade pitch, that covers typically one area traverse (17 GByte), is less than 4 h on a 3.2 GHz pentium processor. The pneumatically averaged flow field is finally measured with a miniature 5-hole cobra probe that uses a tip diameter of only 0.9 mm.

Table 2 Typical error bandwidth of the selected probes for a flow Mach number of Ma=0.15

Probes	α (deg)	β (deg)	C_{pt} (%) Dyn. Head	C_{ps} (%) Dyn. Head	Ma (%)
FRAP	0.3	0.5	3%	5%	3%
5-Hole	0.3	0.3	2%	3%	1%

Probe Measurement Plane. The time-varying secondary flow field and the associated vortical system at the rotor exit plane are measured with detailed probe area traverses in the first stage exit plane in area I as shown in Fig. 2.

A typical spatial resolution of the measurement grid for a FRAP or 5-hole probe consists of 31 grid points per radial traverse (hub to tip) and 21 traverses at equidistant circumferential positions per blade pitch, resulting in 651 grid points. The temporal resolution is 108 samples per blade passing period, which leads to a measurement set of nearly 70,000 data points for one blade pitch.

Results

The measurement results of the steady and time-resolved flow field are shown in this section. The comparison of the pneumatic (5-hole) and time-averaged (FRAP) result is given as pitchwise mass-averaged flow profiles as a function of blade span for the absolute total pressure C_{pt} and the stator incidence angle $\Delta\alpha$ relative to the blade design data.

The second section focuses on the unsteady interaction of the rotor hub vortices with the rotor and stator blades. The evolution of the flow field within area (I) is presented as contour area plot for the rotor relative total pressure C_{ptr} and for eight consecutive time steps within one blade passing period. Of particular interest are the associated incidence angles and the level of flow unsteadiness.

The stochastic part of the FRAP pressure measurement is further analyzed and expressed in terms of the turbulence intensity factor Tu_p (see Ruck [11] and Koeppel [12]). The stagnation pressure P^0 in the flow field is similar to the center hole pressure P_1 of a virtual-four sensor FRAP probe. This assumption is representative for a probe relative flow yaw angle variation of less than ±10 deg and still acceptable for larger relative flow angles. Based on these assumptions, the turbulence intensity Tu, which is usually derived from hot-wire velocity measurements, is correlated with the random variation of the stagnation pressure Tu_p using inviscid and incompressible flow principles. This concept was

Table 1 Typical operating point of the low speed 2-stage axial research turbine

Rig parameter	Value	Accuracy
Rotor speed	2625 rpm	±1 rpm
Pressure ratio	1.32	±0.02%
Aspect ratio (span/ax.chord)	1.8	···
Blade count (rotor/stator)	42/42	···
Outer tip diameter	0.8 m	±0.05 mm
Mach number Ma (rotor/stator)	0.1/0.35	···
Reynolds number Re (axial chord)	2×10^5	···

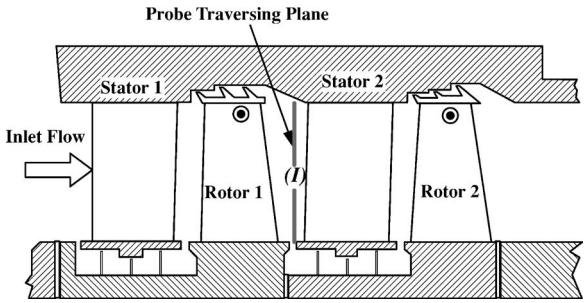

Fig. 2 Probe traversing plane at the exit of the first turbine stage (area I)

verified with the comparison of FRAP measurements (pressure measurement) with LDA (laser doppler anemometry) data for the stochastic velocity field of a centrifugal compressor (Koeppel [12]).

Steady Flow Field at First Stage Exit Plane. The flow field at the exit of the first stage is shown in Fig. 3 for the pitchwise mass-averaged total pressure coefficient C_{pt}. The results of the 5-hole probe are superimposed to the time-averaged flow measurements of the FRAP probes in order to validate the accuracy of the different measurement techniques. The spanwise averaged measurement results for two probe techniques differ by less than 0.001 of C_{pt} (2% of dynamic head) for the entire blade span. A peak difference of 10% dynamic head between the two flow profiles is registered at 28% blade span, which is within the secondary flow dominated area.

The results indicate the presence of considerable secondary flow structures between the rotor hub at 0%–40% of blade span (see circle A). The total pressure varies within 22% of dynamic head due to the effects of the secondary flow vortices on the endwall flow. The re-entering labyrinth leakage flow at the upstream stator hub shroud generates a large nonuniform inlet flow profile into the first rotor blade. The leakage flow rolls-up into a strong rotor hub passage vortex and affects the total pressure distribution at the hub (Schlienger et al. [14]).

The flow profile on the right-hand side of Fig. 3 shows the averaged deviation $\Delta\alpha$ of the absolute flow yaw angle α relative to the design intention α_{design}. The hub passage vortex causes a considerable positive incidence on the stator leading edge of +18 deg at 10% blade span. The over- and underturning of the flow field is due to the induced velocity field of the passage vortex which causes a negative incidence of −8 deg in the upper part of the flow area at 25% blade span. At the blade tip section, a positive incidence of up to 20 deg is measured within 70%–95% of the blade span. This deviation is due to the blade design intention at the tip section.

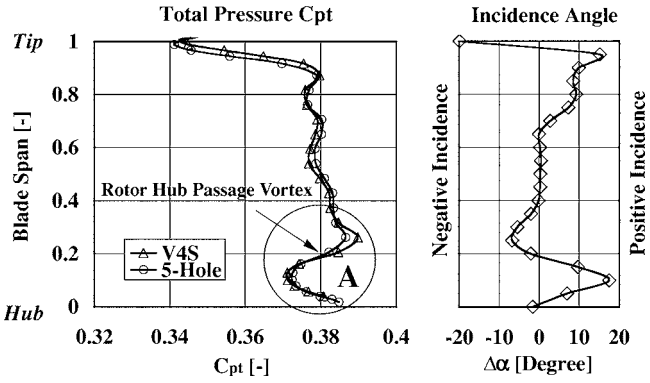

Fig. 3 Total pressure C_{pt} at area I and stator incidence angle Da (relative to design intention)

Unsteady Flow Field at First Stage Exit Plane. The flow field at the rotor hub exit plane (area I) is highly three-dimensional due to the leakage flow at the rotor inlet and exit plane and the high level of flow turning in the blade passage (Langston et al. [15]). These boundary conditions lead to strong secondary flow vortices at the rotor hub, which alters in strength and position during a blade passing event, as seen in this part.

The results of detailed unsteady flow measurements show that the relative motion between the rotor and stator blades affects the convection of the rotor wakes and vortices through the downstream turbine stage. The associated interaction mechanism of the vortices with the wakes, the rotor, and the stator blades is measured in detail and presented in this section. The time-resolved evolution of the flow field is shown for the rotor relative total pressure C_{ptr} and for eight consecutive time steps t/T within one blade passing period T.

The secondary flow field is superimposed onto the contours of the relative total pressure and shown as vector plots (Figs. 4 and 5). The definition of the secondary flow velocities is given in Eq. (1),

$$\mathbf{u}_{\text{sec}} = \mathbf{u}_i - (\mathbf{e}_{\text{mean}} \cdot \mathbf{u}_i)\mathbf{e}_{\text{mean}} \tag{1}$$

The velocity $\mathbf{u}_{\text{sec}}$ is the local secondary flow vector, $\mathbf{u}_i$ the local main flow vector, and $\mathbf{e}_{\text{mean}}$ is the mean area unit vector for the entire flow field at time step t_i. The secondary flow velocity field is recomputed for every new time step. The different vortices are identified in using the local minima of the static pressure, the secondary flow field and the derived vorticity distribution.

Classical secondary flow theories (Hawthorne [16]) assigns the vortical structure on top of the passage vortex to the trailing edge vortex that is combined with the vorticity that is developed in the suction surface boundary layer. An other secondary flow model (Goldstein and Spores [17]) associates the vortical structure on top of the passage vortex to the horse-shoe suction side leg vortex.

The measured secondary flow vectors reveal three separate vortices at different locations in the rotor hub section. The major vortex is the passage vortex and is referenced with *PV*. The small region of high vorticity on top of the *PV* is a combination of horse shoe suction side leg vortex (*HSs*), trailing shed vorticity and suction surface vorticity. A corner vortex (*Cvs*) is found at 5% blade span at the hub of the rotor blade.

The shape of the rotor wake is derived from the measured pitchwise averaged relative flow yaw angle $\beta(r)$ and the axial distance $X(r)$ between the probe and the rotor trailing edge. The corresponding equation for the wake displacement $\Delta_w(r)$ in circumferential direction is given in Eq. (2), with the parameter r as the radial position.

$$\Delta_w(r) = \tan\beta(r) \cdot X(r) \tag{2}$$

The instantaneous position of the rotor trailing edge is known from the blade trigger and the rig geometry. The deformed wake shape $\Delta_w(r)$ is added to the rotor trailing edge geometry, which leads to the sketched shape of the wake.

Discussion of Unsteady Flow Results. The evolution of the different vortices into the downstream stator passage is determined by the relative position of rotor and stator blades and by the stator leading edge potential field, that acts as a radial stagnation line on the evolution and convection of the unsteady flow structures. Any of those rotor indigenous vortices, such as the passage vortex (PV), horse shoe suction side vortex (HSs), or corner vortex (Cvs) will experience a severe bending and stretching as they interact with the downstream stationary stator blades. The unsteady flow measurements that are presented in this paper give a realistic insight into this complex flow mechanism and are dis-

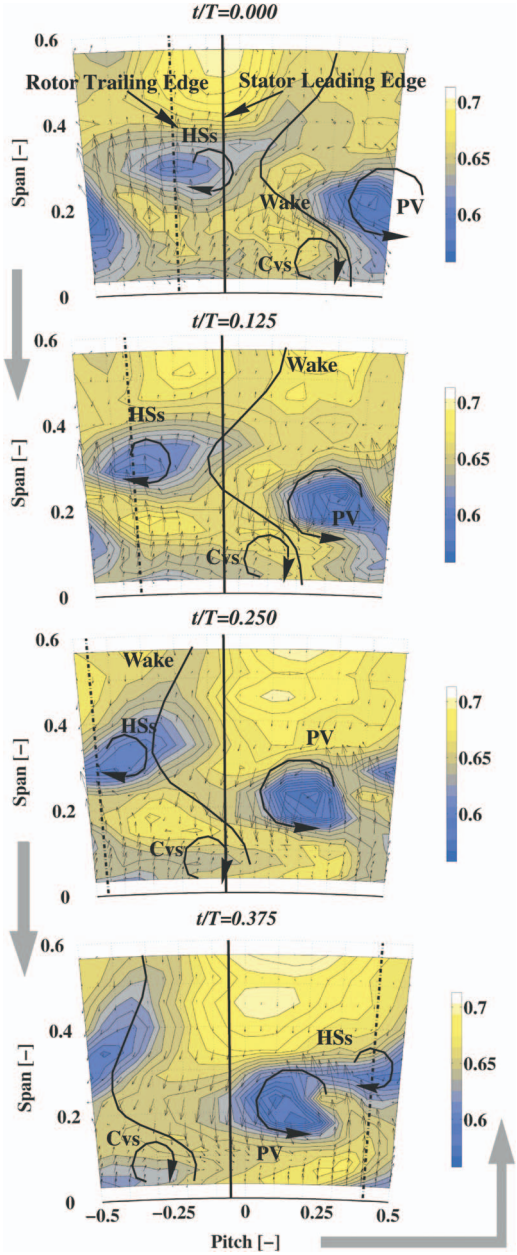

Fig. 4 Relative total pressure and secondary flow vectors at different time steps (area I)

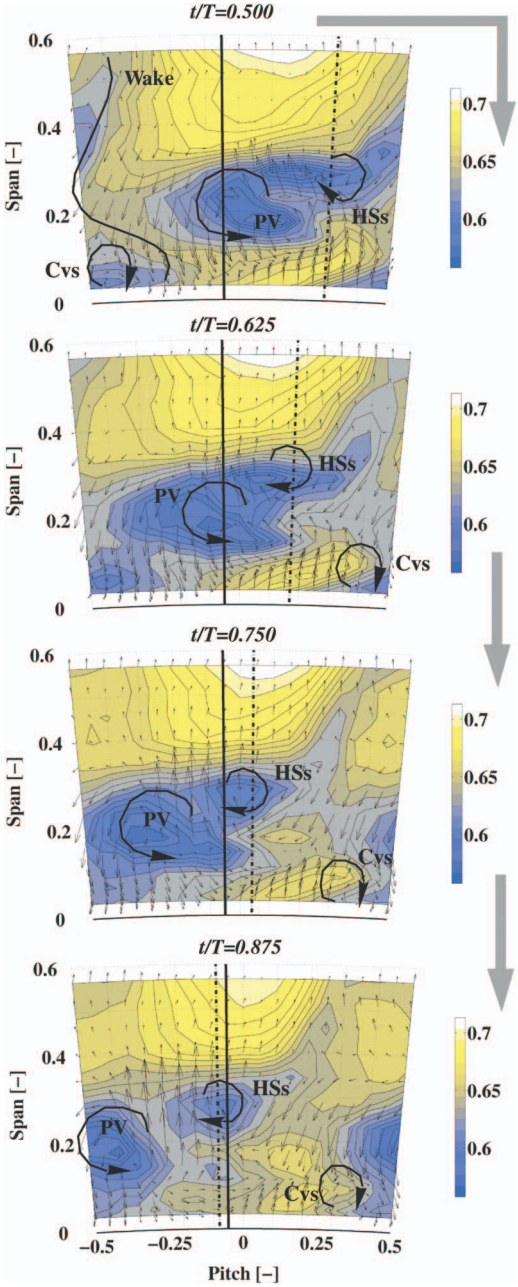

Fig. 5 Relative total pressure and secondary flow vectors at different time steps (area I)

cussed next.

Classical vortex flow theory predicts a static pressure and relative total pressure minimum peak within the core of a vortex tube. This fact is used, together with the secondary flow vectors, to localize the different vortical flow structures within the contour plots of Figs. 4 and 5. With regards to those results, the regions of low relative stagnation pressure are therefore associated to the rotor indigenous secondary flow vortices and the remnants of the upstream first stator endwall flow.

At $t/T=0$ a drop of relative stagnation pressure of 0.08 C_{ptr} (30% relative dynamic head) is found in the core of the passage vortex (PV) when compared to the average level at the hub. This drop remains nearly constant within the entire blade passing period. The size of this local drop in the contour plot varies with time and relative position of the rotor and stator blade rows. The effect of the corner vortex on the stagnation pressure is marginal and is neglected in this discussion.

A flow structure is seen on top of the passage vortex for the entire blade passing period, indicating that this structure is rotor related and associated to the suction side leg of the horse shoe vortex HSs or to the rotor trailing edge vortex. The relative stagnation pressure deficit due to the HSs vortex is half when compared to the passage vortex. The corresponding drop of relative stagnation pressure in the HSs flow structure remains nearly constant within the blade passing period, but the affected flow area doubles for certain time steps ($t/T=0.5-0.75$).

In general, a region of high vorticity often results from high shear and dissipative flow effects that occur within e.g., secondary flow dominated regions within a turbine stage. In particular the strong passage vortex at the rotor exit flow field is held responsible for this result, as found in the experiments for time steps $t/T=0.5$ to $t/T=0.75$. Remarkable is the large area that is covered by the stagnation pressure deficit (70% of blade pitch) at 20% radial span.

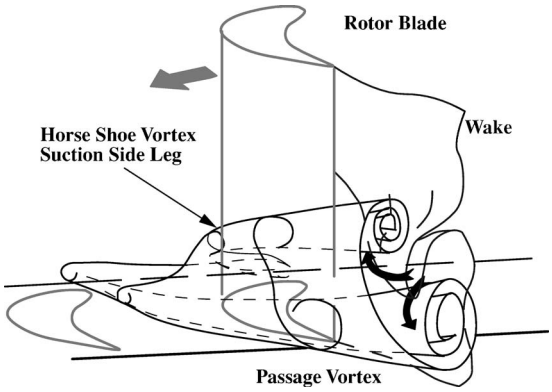

Fig. 6 Schematic of roll-up mechanism of the wake into the secondary flow vortices

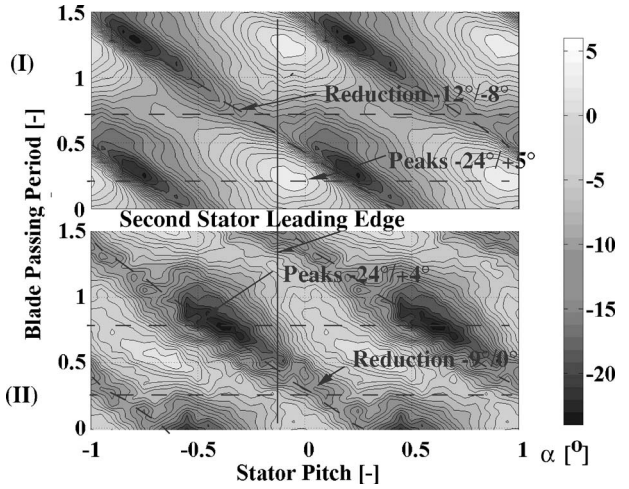

Fig. 7 Space–time diagram for incidence angle Da at 25% rotor blade span (underturning) (I) 0% stator–stator/(II) 50% stator–stator

Additional analysis of the unsteady 3D flow data indicates an increase of 220% of pitchwise averaged streamwise vorticity at a radial height of 0.15 between $t/T=0.25$ to $t/T=0.75$ (Schlienger [13]). This dramatic increase of streamwise vorticity originates from a streamwise stretching of the dominant rotor passage vortex tubes and from the periodic shedding of high vorticity that is generated in the upstream first stator endwall flow field and convects downstream through the first rotor blade row into the measurement volume.

Apart of the vortices that influence the stagnation pressure distribution at the rotor exit, the wake layer also contributes to a loss of stagnation pressure. The wake and its shape is identified in the contour plots of Figs. 4 and 5 and marked by a solid line when using Eq. (2). The shape of the wake is influenced by its proximity to the passage vortex that induces a secondary flow velocity field on to the main flow. The radially aligned wake layer is skewed around the streamwise axis and rolled up into the vortical system at the rotor hub the closer the wake approaches it. High loss fluid is entrained from the wake layer into the endwall secondary flow field as shown in Fig. 6.

The identified vortices interact with the radial vorticity filaments of the rotor wake layer and redistributes high loss fluid in the hub area of the rotor blade row. At times, the wake does not exist as a measurable quantity ($t/T=0.5-0.75$) as it is entrained by the streamwise vortical flow structures. The downstream stator potential field affects, through a change of the rotor exit velocity field, the convection of the upstream rotor indigenous secondary flow and wake structures into the downstream stator blade passage.

Influence of Upstream Stator Flow Field. The secondary flow structures from the first stator blade row are shed into the downstream rotor passage, which affects the formation of the rotor indigenous vortices. The resulting flow structure at the rotor exit faces the downstream second stator blade row with its potential pressure field. The stagnation pressure distribution and the incidence angles in the rotor exit plane depend on the relative position of the first and second stator blade rows (clocking effect). A possible way to assess the influence of stator clocking on the unsteady flow field in the measurement area is by shifting the first stator blade row by half a stator pitch relative to the second stator. This way, the different flow structures are forced to interact at different time instances and positions with the downstream second stator. Any differences of the unsteady flow field for both cases are then associated with the effect of stator clocking. This procedure reveals best the nature of the interaction mechanism and quantifies those differences of incidence angles and relative total pressure due to clocking.

The initial configuration with the axially aligned first and second stator blades are defined as 0% stator–stator case, the second case with the half blade pitch shift of the first stator blade row as 50% stator–stator, respectively. Figure 7 shows the space–time diagram for both configurations for the incidence angle $\Delta\alpha$ at 25% blade span. The flow at 25% span is underturning by −8 deg on average, as seen in Fig. 3. The influence of the rotor relative flow field is visible as inclined contour pattern that is parallel to the dashed lines. The influence of the stator stationary flow field is visible as contour pattern that is perpendicular to the stator pitch axis.

For $t/T=0.25$ the peak incidence reaches a level of −24 deg and +5 deg close to the second stator leading edge at 0 and 0.2 stator pitch. For $t/T=0.75$, those peaks are considerably reduced down to −12 deg and −8 deg. The previous analysis of the measured data showed a maximum deficit of relative stagnation pressure for this time step. Hence, at $t/T=0.25$ the secondary flow field is mainly defined by the rotor indigenous vortices, in particular the passage vortex, that leads to the largest variation of the incidence angle. At $t/T=0.75$, the shedding of the upstream first stator secondary flow field occurs and destroys the strong secondary flow structure at the rotor hub, which reduces the pitchwise variation of incidence angle from 29 deg down to 4 deg. Such a low variation of incidence angle would be positive for the stator blade design. But this beneficial stabilizing effect goes in parallel with a drop of relative stagnation pressure that reduces blade performance and stage efficiency.

The incidence peaks are shifted by 50% in circumferential direction when clocking the first stator by half a blade pitch, as seen in Fig. 7(II). The peak values of positive and negative incidence remain in the same order of magnitude as for case (I). A reduction of incidence angle implies a reduction of over- and underturning of the flow field and thus less secondary flow velocity, which is equivalent to a weakened rotor hub passage vortex. This effect is pronounced in case (I) at $t/T=0.75$ and in case (II) at $t/T=0.25$, which is when the remnants of the shed first stator secondary flow structures passes the measurement area.

Figure 8 shows the corresponding space-time diagram for the relative total pressure C_{ptr} at 25% span. The first comparison of the contour plot for case (I) and case (II) shows a remarkable difference of stagnation pressure variation for the baseline and the clocked turbine stage configuration. With aligned first and second stator blades (case I) the stagnation pressure varies within 0.68 and 0.56 of C_{ptr}, whereas for case (II) there is a variation of within 0.68 to 0.52, which is equivalent to 63% of the relative dynamic head.

The remnants of the shed first stator secondary flow field

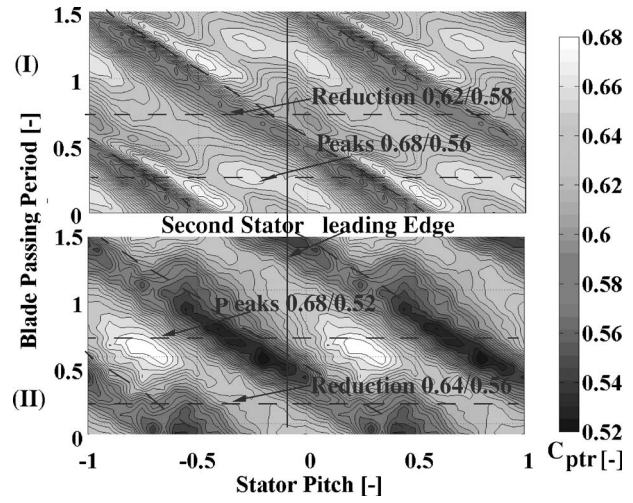

Fig. 8 Space–time diagram for relative total pressure coefficient at 25% blade span (I) 0% stator–stator/(II) 50% stator–stator

crosses the rotor exit plane at $t/T=0.75$ in case (I) and $t/T=0.25$ for case (II). The stagnation pressure contours for case (I) suggest less variation when compared to case (II). This means, that the periodic shedding of the first stator secondary flow structures onto the downstream stator blade are generating high stagnation pressure variations as they convect in between the second stator leading edges at half a blade pitch. In case, that those structures hit the second stator leading edge (case I), the stagnation pressure variation remains moderate. The stator blade potential pressure field reduces the flow unsteadiness by enforcing an acceleration and deceleration effect on the velocity field at the rotor exit plane, as seen in the comparison of Fig. 8 (I) and (II). The results suggest, that the influence of the shed upstream stator flow on the vortex-wake-blade mechanism mainly affects the peaks of unsteady relative total pressure variation rather than the peaks of incidence angle in front of the stator blade.

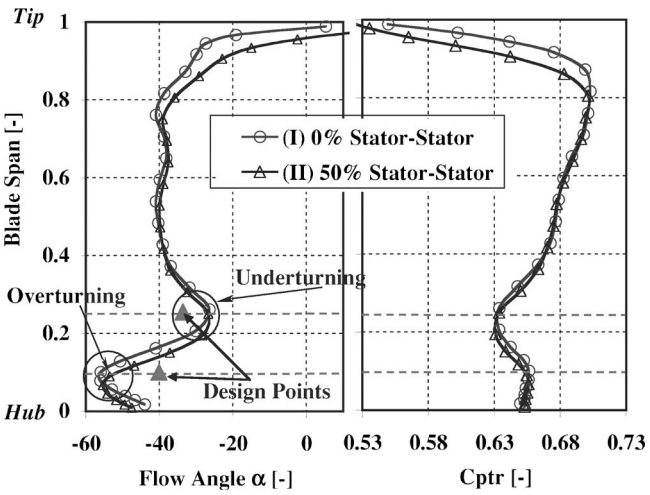

Fig. 9 Effects of stator–stator clocking on mass-averaged flow profiles (at first rotor exit)

The comparison of the pitchwise mass averaged steady flow profiles for the absolute flow angle α and relative stagnation pressure C_{ptr} is shown for both clocking positions in Fig. 9. The time-averaged incidence angles and the relative total pressure do not differ between the two cases (I) and (II) at both 10% and 25% blade span. Although the space–time diagrams (Figs. 7 and 8) showed measurable differences of the instantaneous values, the time-mean values do not.

This surprising result suggests that the interaction mechanism of the observed flow features, even though they occur at different time instances and locations, remains primarily kinematic with no influence of the time averaged values. This important conclusion implies that stator clocking does not generate any effects (positive or negative) that alter the averaged flow field in front of the second turbine stage.

The analysis of the unsteady flow data is summarized in Tables 3 and 4. The steady flow field shows no considerable differences at the hub section within the area of the rotor hub passage vortex dominated flow area between 0%–40% blade span. The result shows a minimal radial migration of the rotor hub vortex towards the hub as a result of the shifted upstream first stator hub endwall flow field.

It is concluded, that the shed vortices from the upstream first stator hub secondary flow field influence the pitchwise variation of unsteady incidence angles and relative stagnation pressure but leaves the time-averaged flow profiles unaffected. The over- and underturning effect at the rotor hub is therefore mainly a result of the rotor indigenous passage vortex, that induces this strong secondary velocity field on the main flow.

Pitchwise Mass-Averaged Unsteady Flow Profiles. The previous section showed an influence of the first stator secondary flow field on the unsteady flow field in the downstream rotor exit area. Stator clocking did not influence time-mean flow profiles but obviously has an effect on the unsteady flow profile distribution as shown in this section.

The results of time-resolved flow field measurements are in general presented as animated flow fields. Alternatively they could be expressed as pitchwise mass-averaged space–time diagrams as

Table 3 Summary of incidence angles $\Delta\alpha$ on second stator blade row for 25% and 10% blade span (I) 0% stator–stator/(II) 50% stator–stator

Blade span	Design α (deg)	Mean (I/II) $\Delta\alpha$ (deg)	Max. (I/II) $\Delta\alpha$ (deg)	Min. (I/II) $\Delta\alpha$ (deg)
25%	−34	−8/−7.9	−3.6/2.9	−23/−24
10%	−40	15.4/16.2	28/26.4	8.1/2.9

Table 4 Summary of relative total pressure C_{ptr} at rotor exit plane I for 25% and 10% blade span (I) 0% stator–stator/(II) 50% stator–stator

Blade span	Mean (I/II) C_{ptr}	Max. (I/II) C_{ptr}	Min. (I/II) C_{ptr}
25%	0.63/0.63	0.68/0.68	0.56/0.52
10%	0.66/0.65	0.67/0.65	0.61/0.59

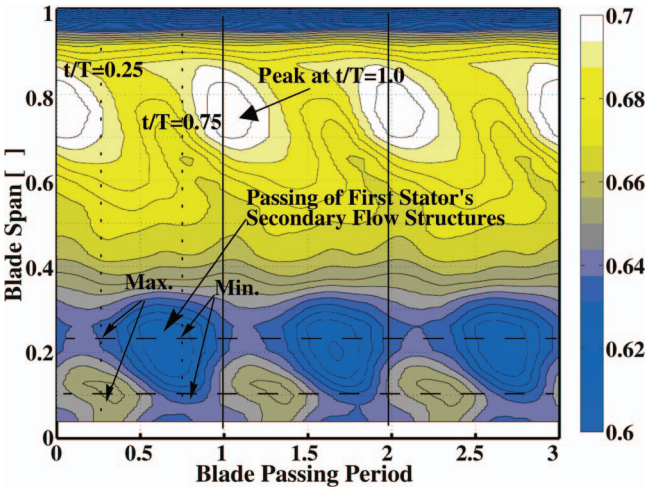

Fig. 10 Pitchwise mass-averaged space–time diagram for relative total pressure C_{ptr} for area (I)

shown in Figs. 10 and 11. The measured data for the flow area (e.g., flow yaw angle) is pitchwise mass-averaged for each timestep t_i and given as a function of blade span r. The result is a space–time diagram for a given number of blade passing periods. An example is shown in Fig. 10 for the relative stagnation pressure C_{ptr} at the rotor exit plane of area I. The results of three consecutive blade passing events (phase lock averaged data) are plotted versus the blade span for the selected flow parameters. The contour lines for a steady flow field (e.g., from 5-hole probe measurements) would show contours that are parallel to the time axis. The identified fluctuations of C_{ptr} along the time axis are thus a result of unsteady flow effects and are evaluated on the basis of the proposed diagram type.

The two time steps for $t/T=0.75$ and $t/T=0.25$ are shown as dotted lines on the contours of Fig. 10. The presence of secondary flow vortices at the rotor hub influences the relative total pressure as seen at 25% blade span (underturning).

With increasing time, the relative total pressure drops from a peak of 0.64 at 25% blade span and $t/T=0.25$ down to 0.61 at $t/T=0.75$ (11% of relative dynamic head). A similar drop is observed at 10% blade height (overturning).

At 40% blade span, the relative stagnation pressure remains nearly constant over time. The rotor blade loading is therefore constant and thus not affected by secondary flow vortices from the

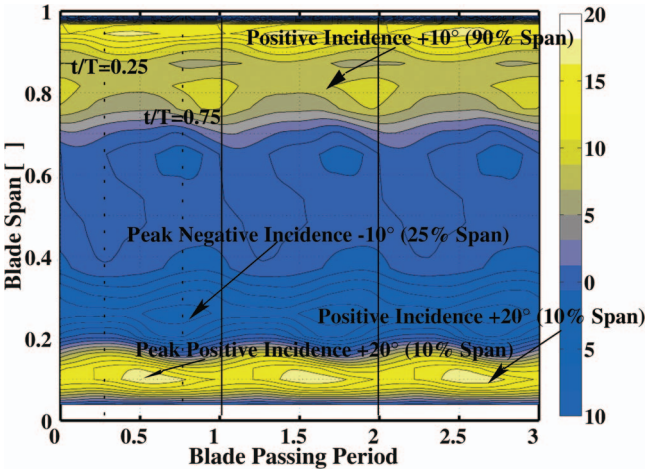

Fig. 11 Pitchwise mass-averaged space–time diagram for incidence angle $\Delta\alpha$ (relative to design)

first rotor or upstream stator flow field. The time-resolved flow measurements show a massflow variation of ±0.6% of the overall massflow for one blade passing event, which is equivalent to a quasi-steady operating point of the turbine stage. The temporal variation of C_{ptr} at the rotor hub (dashed lines) is therefore related to the remnants of the first stator secondary flow field in the rotor exit area and to the interaction effects of the rotor related secondary flow vortices with the wake and the downstream stator blade profiles.

At the tip section of the rotor exit plane a variation of 0.02 C_{ptr} is found at 80% radial span, which is equivalent to 8% of relative dynamic head. This variation is either due to the interaction of the rotor wake with the downstream stator blade row or it results from the shed upstream first stator tip passage vortex. The evaluation of the corresponding contour plot for the clocked turbine stages shows a temporal shift of the observed peak, which associates this peak to the shed flow structure of the first stator rather than to the wake–blade interaction.

The measured variation of total pressure (Fig. 10) is associated with the time-resolved incidence angle $\Delta\alpha$ for three blade passing events, as shown in Fig. 11. The incidence angle is defined here as the angle between the measured instantaneous pitchwise averaged absolute flow angle α and the design intention for the stator blade.

The contour plots of Fig. 11 shows nearly zero incidence on the stator leading edge within the midspan area (between 40%–70% of blade span). The overall unsteady fluctuation of pitchwise mass-averaged incidence angle is considered as moderate and reaches a fluctuation amplitude of ±3 deg of absolute incidence angle at certain blade span positions during one blade passing event. The measured variation is equivalent to nearly 5% of rotor blade loading. The major impact is seen at the endwalls at both hub and tip. The strong secondary flow hub vortices in the rotor passage causes an average negative and positive incidence angle of up to −10 deg with ±3 deg of variation (at 25% span) and at 10% span an incidence angle of +15 deg and a variation of ±3 deg at the rotor hub. The tip section shows a nearly constant positive incidence of +10 deg relative to the blade design at 90% blade span.

Analysis of Stochastic Pressure Signal

The turbulence level in the main flow field can be derived from the time-resolved pressure measurement under certain conditions. If the measured relative probe flow yaw angle remains within ±10 deg, then the derived stagnation pressure $P^0(t)$ is reasonably comparable to the measured center hole pressure $P(t)$ of a 3-sensor or virtual 3-sensor probe. It is assumed that the static pressure fluctuation is of secondary order when compared to the dynamic head variations P_{dyn}. The random signal of the center hole pressure $P'(t)$ is thus representative and equivalent to the random variation of the dynamic head $P'_{\mathrm{dyn}}(t)$ (see Koeppel [12]). A turbulence intensity level Tu_p is introduced that relates the stochastic pressure variation $P'(t)$ to the dynamic head pressure $P_{\mathrm{dyn}}(t)$ according to Ruck [11].

$$\mathrm{Tu}_p = \frac{1}{2} \cdot \frac{\sqrt{\overline{P'^2}}}{\overline{P_{\mathrm{dyn}}}} \tag{3}$$

The derived turbulence level is assumed to be isotropic ($u'=v'=w'$) and is only valid for incompressible flows. The dynamic head P_{dyn} is derived from the probe measurements and calibration model and finally phase lock averaged in order to obtain the deterministic part of the dynamic head.

The introduced turbulence level is derived for the exit flow field of the first rotor hub section in order to evaluate the distribution of random unsteadiness at the rotor hub. In the work of Binder et al. [5] an area of high unsteadiness is observed at the blade pressure side at the inlet to the rotor blade where the upstream stator passage vortex interacts with the rotor blade leading edge.

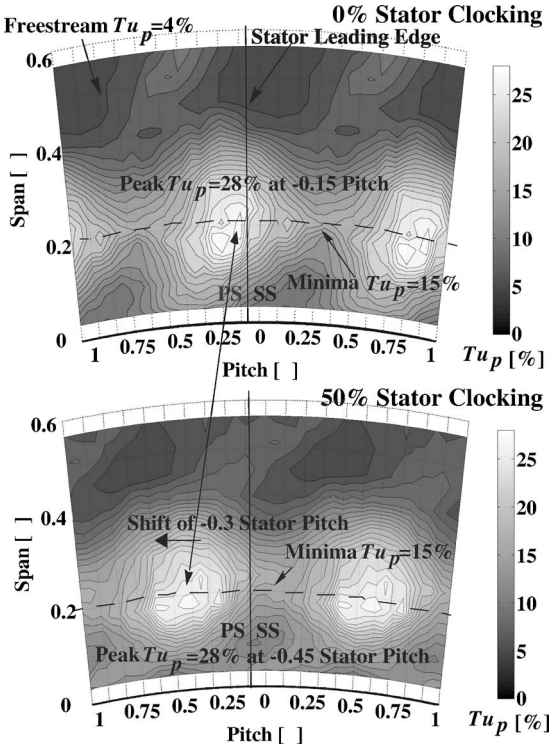

Fig. 12 Time-averaged turbulence level Tu_p of dynamic head at exit of first rotor for 0% stator clocking (baseline) and 50% stator clocking

This level of unsteadiness is also observed in the present analysis of the Tu_p level and shown in Fig. 12 as a time-averaged contour plot at the rotor hub section. The data analysis has been repeated for the clocked version (case II) and shown bellow the baseline contour plot. A freestream turbulence of Tu_p=4% is measured for both configurations (case I and II), which is representative for turbulence levels at the exit of first turbine stages.

The secondary flow dominated area between 10% and 35% blade span shows a very high averaged turbulence level of up to 28% due to the influence of the rotor hub passage vortex and the remnants of the first stator's secondary flow field at the rotor exit. The position of the second stator leading edge is sketched as a solid line at −0.1 blade pitch. A high level of random unsteadiness of +28% Tu_p is identified at the stator blade pressure side whereas a drop of Tu_p down to 15% is observed at half the blade pitch at 20% blade span.

In both cases (baseline and clocked version), the turbulence peak remains at a constant level of 28% Tu_p. The average turbulence level at 10% blade span shows a moderate difference of +10% versus +15% of Tu_p as a result of the stator clocking. However, the turbulence peak of 28% is shifted by only 30% blade pitch in negative circumferential direction when clocking the first stator blade row by half a blade pitch. The observed reduced circumferential shift of the turbulence peak (30% instead of 50%) suggest the following conclusions. The turbulence peak is primarily influenced by the periodic appearance of the shed first stator secondary flow structures that convect through the measurement volume. Clocking the first stator blade row implies a clocking of its endwall secondary flow field and as such a clocking of the area of high unsteadiness in the downstream flow field. The fact that the turbulence peak has only shifted by 30% blade pitch instead of half a blade pitch is surprising.

Conclusions

This paper has shown the key effects of the interaction between the rotor wake, the turbine blades, and the secondary flow vortices that are formed in the rotor and stator blade passages. The characteristic of the unsteady flow field at the rotor hub exit is primarily a result of the interaction between the rotor indigenous passage vortex and the remnants of the secondary flow structures that are shed from the first stator blade row. The clocking of the first stator blade row does not affect the time averaged flow profiles but clearly influences the circumferential positions of the peak values for the relative stagnation pressure, the incidence angles and the stochastic fluctuations of the dynamic head at the rotor exit. The strength of those effects have a potential to influence the formation of secondary flow structures in the downstream blade rows. Finally, the measurements reveal an interesting mechanism between the passage vortex and the wake, that is rolled up into the secondary flow vortical system at the rotor hub, as a result of the induced secondary velocity field of the passage vortex.

Acknowledgment

The investigations were conducted as part of the joint research program "500 MW auf einer Welle AG Turbo II." The work was supported by the German Federal Ministry of Economy (BMWI) under file Nos. 0327060D and 0327060F. The authors gratefully acknowledge AG Turbo, Alstom Power, and Rolls-Royce Germany for their support and permission to publish this paper. The authors would like to express their gratitude to Dr. Erik Janke and Dr. Helmut Richter of Rolls-Royce Germany for their support during this phase of the research project.

Nomenclature

C_{ps} = static pressure coefficient
C_{pt} = absolute total pressure coefficient
C_{ptr} = relative total pressure coefficient $C_{ptr}=(P^0_{\text{rel,local}}-P_{\text{Turbine out}})/(P^0_{\text{Turbine in}}-P_{\text{Turbine out}})$
$\vec{e}$ = mean unit vector (area)
P^0_{rel} = relative total pressure (Pa)
P' = random part of pressure signal (Pa)
P_{dyn} = dynamic head (Pa)
t = time (s)
T = blade passing period (s)
Tu_p = turbulence level of stagnation pressure (%)
U = rotor speed (m/s)
$\vec{u}_{\text{sec}}$ = local secondary flow vector (m/s)
$\vec{u}_{\text{i}}$ = local main flow vector (m/s)
v = velocity (m/s)
X = axial distance (trailing edge to probe)
Δ_w = circumferential wake displacement
α = absolute flow yaw angle (deg)
β = relative flow yaw angle (deg)
$\Delta\alpha$ = deviation relative to design intention (deg)

References

[1] Denton, J. D., 1993, "Loss Mechanisms in Turbomachines," The 1993 IGTI Scholar Lecture. J. Turbomach., **115**, pp. 621–656.
[2] Sharma, O. P., Butler, T. L., Joslyn, H. D., and Dring, R. P., 1985, "Three-Dimensional Unsteady Flow in an Axial Flow Turbine," AIAA J., **1**, pp. 29–38.
[3] Miller, R. J., Moss, R. W., and Ainsworth, R. W., 2003, "The Development of Turbine Exit Flow in a Swan-Necked Inter-Stage Diffuser," ASME GT-2003-38174, Atlanta, Georgia.
[4] Hodson, H. P., 1985, "Measurements of Wake Generated Unsteadiness in the Rotor Passages of Axial Flow Turbines," ASME J. Eng. Gas Turbines Power, **107**, pp. 337–344.
[5] Binder, A., Förster, W., Mach, K., and Rogge, H., 1986, "Unsteady Flow Interaction Caused by the Stator Secondary Vortices in a Turbine Rotor," ASME 1986-GT-302.
[6] Boletis, E., and Sieverding, C. H., 1991, "Experimental Study of the Three-Dimensional Flow Field in a Turbine Stator Preceded by a Full Stage," ASME J. Turbomach., **113**, pp. 1–9.

[7] Chaluvadi, V. S. P., Kalfas, A. I., Hodson, H. P., Ohyama, H., and Watanabe, E., 2003, "Blade Row Interaction in a High Pressure Steam Turbine," ASME J. Turbomach., **125**, pp. 14–24.
[8] Behr, T., Porreca, L., Mokulys, T., Kalfas, A. I., and Abhari, R. S., 2004, "Multistage Aspects and Unsteady Effects of Stator and Rotor Clocking in an Axial Turbine with Low Aspect Ratio Blading," ASME GT-2004-53612, Vienna, Austria.
[9] Chaluvadi, V. S. P., Kalfas, A. I., and Hodson, H. P., 2003, "Generating a Vortex to Study Vortex Interaction in an Axial Flow Turbine," 5th European Conference on Turbomachinery 2003, Conference Proceeding, pp. 1029–1038.
[10] Kupferschmied, P., Köppel, P., Gizzi, W. P., and Gyarmathy, G., 2000, "Time-Resolved Flow Measurements with Fast-Response Aerodynamic Probes in Turbomachines," Meas. Sci. Technol., **11**, pp. 1036–1054.
[11] Ruck, G., 1989, "Ein Verfahren zur instationären Geschwindigkeits- und Turbulenzmessung mit einer pneumatisch messenden Keilsonde," Mitteilung des Instituts No. 33, University of Stuttgart, Germany.
[12] Koeppel, P., 2000, "Instationäre Strömung in Turbomaschinen: Analyse Zeitabhängiger Sondenmessungen," Ph.D thesis Nr. 13500, ETH Zurich, Switzerland.
[13] Schlienger, J., 2003, "Evolution of Unsteady Secondary Flows in a Multistage Shrouded Axial Turbine," Ph.D. thesis, No. 15230, ETH Zurich, Switzerland.
[14] Schlienger, J., Pfau, A., Kalfas, A. I., and Abhari, R. S., 2003, "Effects of Labyrinth Seal Variation on Multistage Axial Turbine Flow," ASME Atlanta 2003-GT-38270.
[15] Langston, L. S., Nice, M. L., and Hooper, R. M., 1977, "Three Dimensional Flow Within a Turbine Cascade Passage," ASME J. Eng. Power, **99**, pp. 21–28.
[16] Hawthorne, W. R., 1955, "Rotational Flow Through Cascades," Q. J. Mech. Appl. Math., **8**, Pt. 3, Sept., pp. 266–279.
[17] Goldstein, R. J., and Spores, R. A., 1988, "Turbulent Transport on the Endwall in the Region Between Adjacent Turbine Blades," ASME J. Heat Transfer, **110**, pp. 862–869.